Solar Energy Materials & Solar Cells 161 (2017) 149–156

Contents lists available at ScienceDirect

Solar Energy Materials & Solar Cells

journal homepage: www.elsevier.com/locate/solmat

Photon and carrier management design for nonplanar thin-film copper indium gallium selenide photovoltaics

Colton R. Bukowsky[a,*], Jonathan Grandidier[a,b], Katherine T. Fountaine[a,c], Dennis M. Callahan[a,d], Billy J. Stanbery[e,f], Harry A. Atwater[a,*]

[a] California Institute of Technology, 1200 E. California Drive, Pasadena, CA 91125, USA
[b] Jet Propulsion Laboratory, 4800 Oak Grove Dr., Pasadena, CA 91109, USA
[c] NG Next, Northrup Grumman Aerospace Systems, One Space Park Dr., Redondo Beach, CA 90278, USA
[d] Charles Stark Draper Laboratory, Inc., 555 Technology Square, Cambridge, MA 02139, USA
[e] HelioVolt Corporation, 6301 E Stassney Ln, Austin, TX 78744, USA
[f] Siva Power, 5102 Calle del Sol, Santa Clara, CA 95054, USA

ARTICLE INFO

Keywords:
Solar cells
Thin film
Light trapping
CIGS
Nanotextured

ABSTRACT

Nonplanar structured photovoltaic absorber design has potential to achieve high solar cell efficiency with significantly reduced material use. We report optoelectronic simulations that highlight photon and generated carrier management opportunities for improvement of thin film $Cu(In_xGa_{1-x})Se_2$ (CIGS) device performance. Structures realized via either self-assembly or patterning via nanoimprint lithography, and also a combination of both are predicted to exhibit significant increases in short circuit current density and open circuit voltage simultaneously. The structures investigated include: 1) self-assembled nonplanar structures that strongly scatter incident light and enhance carrier generation near regions of high electric potential, 2) lithographically-patterned embedded periodic dielectric structures, 3) planar dielectric layers that separate the CIGS absorber from the molybdenum back-contact via reduced-area contacts that minimize optical and electronic losses, 4) a combination of these for combined effects. We find that the self-assembled nonplanar CIGS cells with 700 nm planar equivalent thickness, combined with dielectric separation layers yield increases in short circuit current density and open circuit voltage up to 3.4 mA cm^{-2} and 29 mV, respectively. The absolute efficiency increases from 15.4% to 18.1%, compared to the predicted efficiency for planar CIGS thin film cells of equivalent thickness. The addition of a single layer MgF_2 anti-reflection coating brings the maximum predicted efficiency up to 19.7% for randomly textured devices.

1. Introduction

Thin-film solar cells have been researched as alternatives to crystalline silicon solar cells for decades due to high efficiencies greater than 20% and the intrinsic benefits of thicknesses on the order of microns, such mechanical flexibility and a variety of substrate options. Typically, CIGS photovoltaic devices are between 1 – 3 μm thick, allowing the majority of incident sunlight to be absorbed. Reducing the thickness of devices below 1 μm is desirable to increase production throughput capacity while reducing the materials cost associated the rare-earth metal indium, which is also highly in demand for large area applications by the flat-panel display industry. Reducing thickness would also decrease the number of minority carriers lost to bulk recombination, thereby increasing the voltage of devices [1]. However sub-micron cells cannot absorb all incident photons in a traditional planar architecture, and the benefits of reduced bulk recombination are lost due to surface recombination at the back-contact. Here, we demonstrate that nanophotonic structures could address both of these issues, leading to efficiencies unattainable by planar devices with the same electronic qualities.

Light management by incorporation of randomly textured microstructures or nanostructures has been extensively investigated for crystalline silicon, amorphous silicon, and GaAs photovoltaics [2–7], but such approaches have not been as extensively applied to polycrystalline thin-film compound materials and devices, such as CIGS, CdTe, and Cu_2ZnSnS_4. [8,9] Here, we explore the underlying mechanisms of unexpectedly high absorption in random textures that were seen experimentally by the Heliovolt Corporation and compare them to other popular light trapping structures for thin-film photovoltaics [10–12]. Our simulation approach is uniquely able to extract differences

* Corresponding author.
E-mail addresses: cb@caltech.edu (C.R. Bukowsky), haa@caltech.edu (H.A. Atwater).

http://dx.doi.org/10.1016/j.solmat.2016.11.008
Received 15 June 2016; Received in revised form 4 November 2016; Accepted 6 November 2016
Available online 03 December 2016
0927-0248/

between different structures by holding constituent materials parameters constant, such that performance differences are solely due to device geometry. By building on progress in other materials systems, we identify opportunities for improvement to both the short-circuit current density (J_{SC}) and open circuit voltage (V_{OC}) via coupled optoelectronic simulations.

Many studies of light management in photovoltaics and solar cell architectures have focused on increased light absorption as a design objective with important implications [13,14]. As a first approximation, this type of analysis gives a qualitative indication of how light management can increase cell efficiency. However, coupled optoelectronic modeling in which both full-field electromagnetic simulation of light absorption and scattering is combined with detailed carrier generation, transport, and recombination models results in a more complete picture [15,16]. Accurate modeling of the spatial distribution of generated carriers is important, in addition to increasing overall absorption, because ultimately, the charge carrier collection efficiency directly affects photovoltaic efficiency. Only a full optoelectronic model can quantitatively relate optical absorption enhancement, electronic transport, and photocurrent density enhancement, and highlight electronic transport issues which can be overcome by improved optical design. For example, we observe that randomly textured CIGS absorbers can absorb the majority of the incident spectrum in a film of 700 nm planar equivalent thickness, but generated carriers are lost to parasitic recombination at the nearby back-contact interface. Strategies to overcome these issues are described as well other light trapping schemes for CIGS devices grown via more conventional film synthesis processes. We identify possible CIGS device architectures that enable thinning of the CIGS absorber layer to an equivalent thickness of 700 nm while maintaining or improving the J_{SC} and/or the V_{OC} compared to those of thicker planar devices.

2. Methods

2.1. Optical modeling of CIGS absorbers

Randomly textured CIGS thin film photovoltaic absorbers exhibit a complex film topography that results from a Cu and Se flux assisted recrystallization process, leading to grain coalescence and coarsening as well as void formation via reactive mass transport [10]. These absorber layers were experimentally seen to have exceptional light trapping characteristics, motivating this numerical simulation study of the underlying light trapping mechanisms in comparison to other potential architectures. Experimental corroboration of the device performances predicted by the models herein was rendered impossible by the cessation of Heliovolt's research and development effort. However, the published experimental External Quantum Effciency (EQE) measurements qualitatively match the results herein, leading to the conclusion that our representation is a reasonable approximation of these textured devices [10].

The provided cross-sectional scanning electron microscope (SEM) images of these absorber films were used to construct models for optoelectronic simulations aimed at identifying mechanisms of light trapping. A representative cross-sectional image can be seen in Fig. 1a, which is a CIGS film with equivalent planar thickness of 1.7 μm. This cross section was contrast-thresholded and filtered with imaging software to create a digital representation of the film [17].

The device schematic in Fig. 1b illustrates a simulated device structure that utilizes this absorber film morphology. The device cross section in Fig. 1b includes a 50 nm, CdS conformal window layer, contacted to a CIGS absorber layer to simulate device structure resulting from conformal bath deposition. Voids which occur naturally during the recrystallization process are included in the model, and are consistent with the film morphologies observed in cross-sectional SEM micrographs. The CdS layer is coated with a 150 nm aluminum-doped zinc oxide (AZO) that fills the remainder of the volume and serves as a transparent front contact. The back-contact consists of a 500 nm molybdenum (Mo) planar thin film.

Representative devices cross sections, such as in Fig. 1b, were rendered for full field electromagnetic simulations in two dimensions (2D) with periodic boundary conditions [14]. Electromagnetic simulations using the finite-difference time-domain (FDTD) method were performed with normally incident plane wave illumination; all optical quantities reported here were obtained as polarization averages of the transverse electric and transverse magnetic responses for the films. The absorbed fraction of the incident solar spectrum was constructed from a set of single wavelength electromagnetic simulations that were then power-weighted by the spectral irradiance of the ASTM -AM1.5G solar

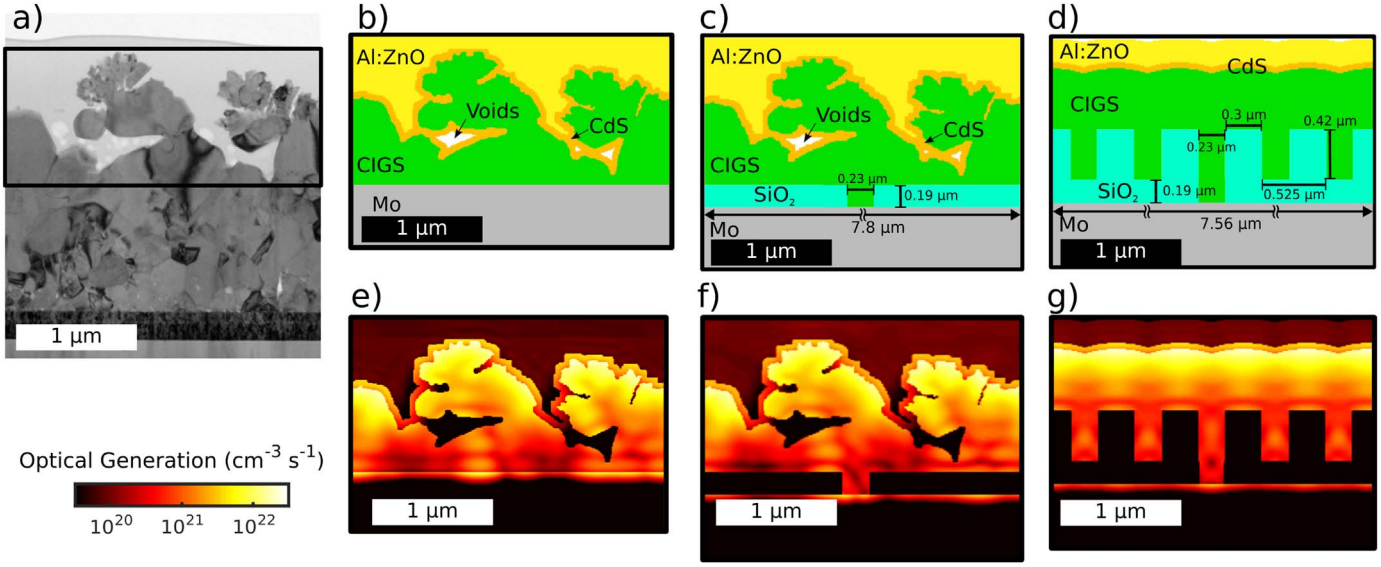

Fig. 1. Simulated Cross-Sections a) A representative SEM of a focused ion beam (FIB) cross section of randomly textured CIGS absorber films is used to define the photovoltaic model for a Mo back-contact device, shown in b). In c), a SiO_2 layer serves to increase reflection and define electrical line contacts, enhancing CIGS film passivation; d) shows a periodic CIGS photonic structure defined by absorber deposition on a patterned SiO_2 layer with electrical line contacts. The optical generation profiles, weighted by the AM-1.5G solar spectrum, for simulated devices from b), c), and d) are shown in e), f), and g).

spectrum. The fractional gallium composition of absorbers in [10] is close to x=0.4, and refractive index data for this composition was used to construct the complex dielectric function for CIGS absorbers in electromagnetic simulations [18]. CdS optical constants are taken from [19], ZnO from [14], and Mo from the Sopra Materials Database [20]. The power absorbed in each material can be calculated from the electric field magnitude and complex refractive index at each mesh point in the simulation. The optical generation rate, G_{opt}, is calculated by

$$G_{opt}(\lambda, \vec{r}) = \frac{\epsilon''(\lambda, \vec{r})|\mathbf{E}(\lambda, \vec{r})|^2}{2\hbar} \quad (1)$$

where ϵ'' is the imaginary part of the material's complex permittivity, $|\mathbf{E}|^2$ is the electric field magnitude, $\vec{r}$ is the position vector, λ is the wavelength, and $\hbar$ is the reduced Planck's constant [14,15]. Spatial maps of charge carrier generation are then used as inputs of the device physics simulations described in the following section [15,21].

2.2. Electronic modeling of CIGS absorbers

The optical generation profiles for all structures depicted in Fig. 11 as well for planar films were input into carrier transport simulations to numerically calculate the steady state EQE and current density-voltage (J-V) characteristics of each device. We took advantage of previously reported transport parameters for CIGS photovoltaics [22], except where explicitly stated herein. While the reader is referred to [22] for specific materials parameters, we explicitly point out two important parameters here. First, the CIGS| Mo surface recombination velocity is set to the thermal velocity, 10^7 cms^{-1}, and represents a worst-case scenario. This is in addition to a Mo|CIGS Fermi-valence band offset of −0.2 eV causing the valence band in the region close to the back-contact bends downward. Second, the defect density model used here more rigorously represents non-uniform lifetimes in regions with strong illumination and depletion, giving a more accurate response than the Shockley-Read-Hall (SRH) recombination model. Still, an instructive estimate of the CIGS bulk minority(majority) carrier diffusion length, as determined by the Einstein relation for diffusivity and the SRH equation of lifetime, is about ~700 nm (~8 μrm) with the parameters used. Our planar device model quantitatively matches closely to Ref. [22]. The slightly lower short-circuit current densities, and correspondingly slightly lower open circuit voltages, between our model and that of Ref. [22] can be explained by the more rigorous treatment of light absorption and local photocarrier generation rate provided by FDTD simulations and the fact that the optical constants used in Ref. [22] were not reported.

This simulation method is general and can be used for any arbitrarily-shaped 2D device cross-section. Absorption in the randomly textured CIGS films was compared to planar thin films (not shown in Fig. 1), CIGS films with dielectric separation layers (Fig. 1c), and CIGS films deposited onto periodic dielectric structures (Fig. 1d). Figs. 1c and 1d show only a subset of the larger structure periodicity defined by line contacts (the 2D approximation to point contacts), with contact periodicity of 7.8 μm and 7.56 μm respectively. Fig. 1f and Fig. 1g depict the total optical generation of those structures, respectively.

3. Results and discussion

3.1. Optical analysis

3.1.1. Absorption in self-assembled randomly textured CIGS films

Looking at the generation map of Fig. 1e immediately highlights two findings from full field electromagnetic simulation: (1) photocarrier generation hotspots in the CIGS absorber, and (2) areas of parasitic absorption in surrounding layers. Areas of high carrier generation are generally close to the randomly textured CdS/CIGS film interface. The randomly textured CIGS surface layer absorbs most of the incident light, suggesting that the underlying 1 μm CIGS film beneath the surface topology in Fig. 1a could be superfluous with respect to light absorption. Fig. 2a shows results for a series of randomly textured CIGS structures with varying underlying bulk film thickness, t (inset), where lighter shades of blue correspond to thinner absorber layers. Typically, in CIGS photovoltaics, absorbing layer thicknesses are on the order of 2 – 3μm [23]. The thickest film simulated in Fig. 2a corresponds to the addition of a 1 μm layer of underlying CIGS material, illustrated by the darkest blue curve, resulting in a CIGS device with a planar equivalent thickness of 1.7 μm, similar to the typical absorber thickness for CIGS. The high absorption of the randomly textured CIGS device is a remarkably constant across the visible and near infrared (NIR) spectrum above the CIGS bandgap, and qualitatively resembles experimentally measured EQE spectra of reference [10], as discussed later. As the underlying CIGS film thickness is varied from 1 μm to 0 μm, the reduction in absorbed photocurrent in CIGS less than 3%. This result indicates an exceptional ability of randomly textured CIGS

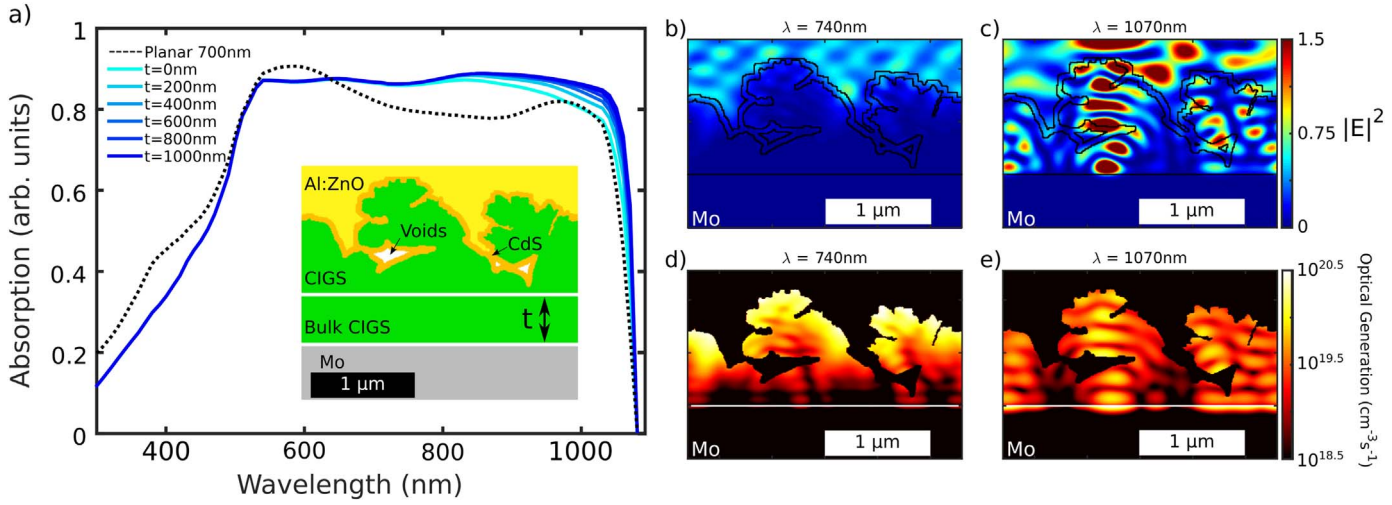

Fig. 2. Randomly Textured Absorbers a) Absorption for CIGS device with a randomly textured absorber. Inset shows thickness, t, of planar CIGS film underlying randomly textured structure, which is varied between 0 μm (light blue) and 1 μm (dark blue). Absorption is nearly constant across the spectrum and weakly dependent on film thickness. In b) and c), magnitude of the polarization-averaged electric field intensity, $|\mathbf{E}|^2$, at λ=740 nm and λ=1070 nm respectively. Structure is outlined with black. In d) and e), optical generation rate; Mo back-contact interface indicated by horizontal white line. (For interpretation of the references to color in this figure legend, the reader is referred to the web version of this article.)

film structures to efficiently scatter and/or absorb light that would be reflected or transmitted by a planar device with equivalent 700 nm CIGS thickness, represented as the black dashed curve in Fig. 2a.

Figs. 2b and 2c show TE and TM averaged electric field intensity, $|\mathbf{E}|^2$, profiles at $\lambda = 740$ nm and $\lambda = 1070$, and Figs. 2d and 2e show the corresponding optical generation rates. These profiles indicate strong light scattering and absorption by the randomly textured CIGS films. Absorption in the planar device begins to decline at wavelengths beyond 600 nm due to increasing reflection, while absorption in the randomly textured CIGS absorbers does not decline until ~740 nm due to the longer optical path lengths and scattering promoted by the texture, as demonstrated in Figs. 2b and 2d. Beyond 740 nm, the randomly textured CIGS begins to transmit light, and a non-zero thickness for the underlying CIGS layer is required for full absorption. In regions of the spectrum where light reaches the Mo back-contact, it is parasitically dissipated in the metal. The significant absorption loss in the Mo is due to its refractive index being relatively well-matched to CIGS, leading to a low reflectivity interface [8,24]. Typically, the metal back-contact in a solar cell should serve as a good back reflector to enable multi-pass absorption, in addition to its role as an electrical contact. However, in a CIGS solar cell, Mo is typically used to create a small to zero Schottky contact to CIGS and for its Na^+ permeability, despite its undesirable optical properties [25,26].

Furthermore, Figs. 2c and 2e indicate field intensity enhancement in the lobes of the CIGS randomly textured structure; these lobes are characterized by their location above a void. The sharp refractive index contrast at the CIGS|CdS|void interface results in reflection back into the absorber material. Thus these lobes effectively act as monolithically integrated low Q resonators. These lobes are also areas of high electric potential, implying that a large fraction of the carriers generated in these regions are collected.

Fig. 3a shows the spectral absorption of each material in the randomly textured CIGS structure with no underlying planar CIGS film (Fig. 1b, 1e) to aid the identification of opportunities for more efficient light management. The solid black curve overlaid onto the absorption spectra represents the simulated EQE, with the difference between absorption and EQE indicating device Internal QE. The most significant fraction of absorption occurs in the CIGS layer (blue). However, at wavelengths shorter than the AZO and CdS bandgaps, CIGS absorption is significantly diminished due to parasitic interband transitions in the CdS and AZO layers. The parasitic absorption at shorter wavelengths accounts for ~11% of the total incident photons above the CIGS bandgap (4.4 mAcm). We note that AZO parasitic absorption here is greater in the randomly textured structure than in a traditional planar design because of the increased total AZO material required to make a conformal front contact here. While light absorbed in the AZO is completely lost, the simulated EQE curve (solid black) shows that some carriers generated in the CdS window layer do contribute to the short circuit current. However, this collection from the CdS is inefficient due to the high defect concentration in the window layer [22]. Optically, a thin AZO layer would be ideal, but electronically, a thin AZO layer would incur increased resistive losses. Similarly, further thinning of the CdS could also be detrimental, causing pin holes and shunts among other transport-related issues [23,27]. Use of wider band gap heterojunction window layer materials is a potential alternative to minimize photocurrent lost in CdS, and is currently under investigation [26,28].

Fig. 3b shows the material parsed absorption for a textured CIGS device with t = 1 μm. The absorption response in the blue wavelengths is the same because the device is not optically thin. Unsurprisingly, the major difference between the thick device and the thin device is a reduced portion of NIR spectrum is absorbed by the Mo back-contact. The solid black curve overlay represents the simulated EQE of the thicker device, which has increased proportional to the reduced absorption in the Mo back-contact in the NIR. Additionally, the dashed black curves show experimental data from Ref. [10] for comparison.

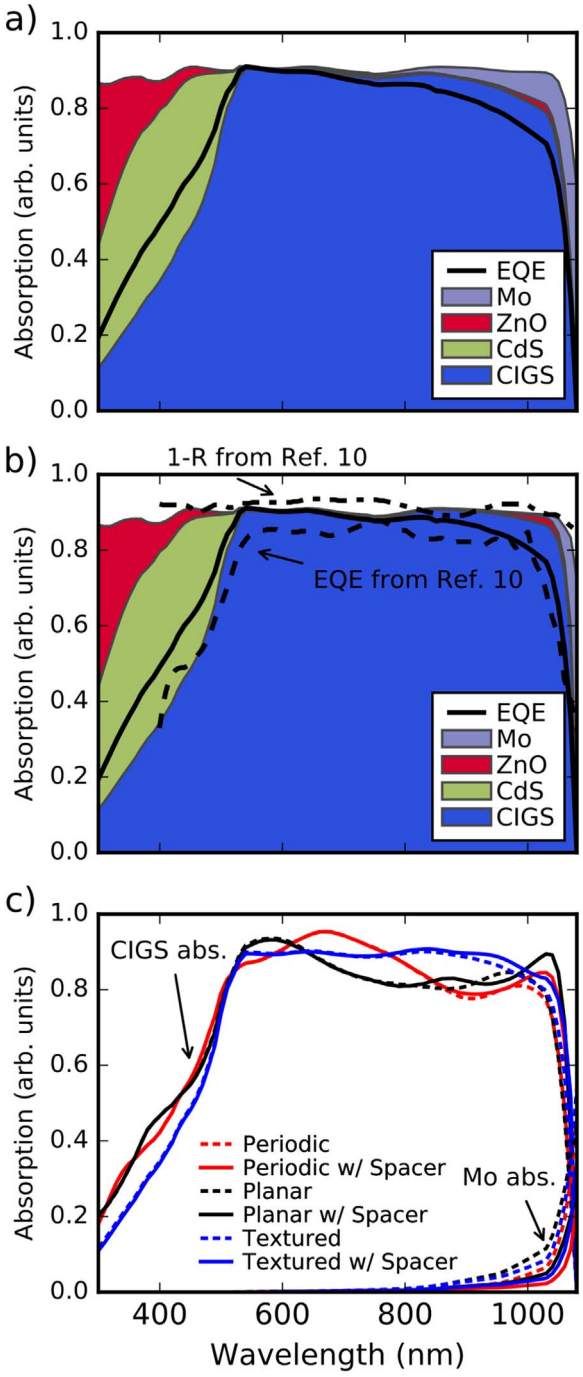

Fig. 3. Absorption in Component Materials a) Materials parsed absorption in a simulated randomly textured device with a planar equivalent of 700 nm, t=0 nm. The black curve overlaid on the plot is the simulated device external quantum efficiency. b) The same as in a, but for t=1000 nm. The 1-R and experimental EQE from [10] are provided in dashed lines for direct comparison to the model here. In c), comparison of CIGS and Mo absorption for different device structures with and without dielectric layers between the absorber and back-contact.

Optically, the 1-reflection (1−R) curve shows that the overall absorption is closely matched. More importantly, the experimental and simulated EQE curves display a reasonably similar behavior. Both EQE curves show a large, flat response across the solar spectrum into the NIR enabled by the strong scattering of longer wavelengths. The difference in the higher simulated EQE curve can be ascribed to using literature values for electronic properties of the material, but the agreement enables us to draw conclusions about the factors that are

most important in structured devices.

Thus as shown in Fig. 3a and b, the other optical loss mechanisms are reflection at the front surface interface and absorption by the Mo back-contact. Front surface reflection losses can be broadly addressed by applying at typical MgF_2 anti-reflection coating (see SI1). The loss in the Mo can be mitigated by appropriate design of dielectric reflection layers to give high refractive index contrast along with promising electronic transport behavior [12], as discussed below.

3.1.2. Thin film and patterned dielectric layers

Parasitic losses in the Mo are difficult to avoid for sub-micrometer absorber layer thicknesses. However, these losses can be reduced by increasing reflectance at the CIGS |Mo interface. A dielectric separation layer with Mo line contacts, as shown in Figs. 1e and 1f, has been proposed to increase reflectance at this interface [29,12,30]. To maximize the reflectance of this new dielectric interface, the dielectric layer should have a low index and its thickness should be designed for destructive interference at wavelengths near the band edge. As an example, low refractive index silica sol gel (n=1.42) layers could be utilized and patterned via nanoimprint lithography [31,32]. Due to the nonplanar film morphology studied here, we optimized this low index layer for absorbed photocurrent using FDTD and partial spectral averaging for all device geometries. This approach more closely resembles experimental results due to the small, random thickness variations of real films [33]. An optimum layer thickness of ~190 nm was found. This low refractive index layer thickness maximizes its reflectance at $\lambda = 1040$ nm, seen as a CIGS absorption peak in Fig. 3c.

Fig. 3c demonstrates the reduction of parasitic Mo absorption and correspondingly increased CIGS absorption due to enhanced CIGS back interface reflectance for the structures depicted in Fig. 1 as well as a planar thin film. First, comparing the dashed black curve and the solid black curve, we see that insertion of the low index layer into the planar structure increases absorption in a planar film slightly at wavelengths where the CIGS is optically thin, beginning around 800 nm. The largest boost in absorption is near the band edge, where the dielectric layer is designed to reflect light back into the CIGS absorber via destructive interference.

Alternatively, periodically ordered structures, such as an array of pillars, can also improve absorption in the CIGS layer (Fig. 1d, 1g). An ordered structure, that has again been optimized for absorbed photocurrent, with a period of 525 nm, a height of 420 nm, and feature width of 300 nm imparts periodic structuring to a conformably deposited CIGS absorber layer. This strongly increases CIGS absorption between 600 nm and 800 nm, seen in the red dashed curve of Fig. 3c, corresponding to the maximum of solar photon flux. This periodic structure has similar anti-reflection properties as the randomly textured absorbers, where the conformal and periodic surface texture preferentially scatters light into the absorber at these wavelengths, seen as the generation by the junction in Fig. 1g [34,35]. Unlike the randomly textured absorber, a periodic structure can be controllably reproduced via methods such as nanoimprint lithography. Augmenting the periodically ordered structures with a 190 nm dielectric layer at the Mo interface gives an additional absorption increase close to the band-edge, exhibited by the solid red curve of Fig. 3c. The overall absorption spectrum closely resembles a superposition of the effects from the two light trapping mechanisms, suggesting multiple strategies can be combined to achieve overall broadband enhancement. A $\frac{1}{4}$ wavelength MgF_2 anti-reflection coating tuned to $\lambda \sim 900$ nm is discussed in Supplementary Information section SI1.

Combining a dielectric reflection layer with randomly textured CIGS absorbers does not result in the same absorption enhancement as with the lithographically patterned and planar films, as seen when comparing the solid and dashed blue curves of Fig. 3c. The reduced enhancement is attributed to the strong scattering of incident light, which inhibits the destructive interference condition within the dielectric layer. Nevertheless, a modest broadband increase in absorption is seen at longer wavelengths where the CIGS absorber is optically thin, beginning around $\lambda = 900$ nm. This corresponds to the fraction of light that is reflected back into the absorber at the CIGS|SiO_2 interface, and can be inferred by comparing the Mo absorption curves of the three architectures without and with dielectric separation layers (dashed versus solid) in Fig. 3c. The dielectric layer clearly decreases the parasitic absorption near the band edge in all cases, verifying the enhanced back interface reflectance.

3.2. Carrier transport analysis

3.2.1. Randomly textured absorbers

The absorbed photocurrent can be determined for optical structures with improved light management, such as the randomly textured CIGS absorbers described here, but the corresponding device transport and electrical performance cannot be predicted from optical models alone. Common assumptions in existing literature on optical modeling of photocurrent enhancement include unity or constant internal quantum efficiency, neglecting wavelength and/or spatially dependent collection probabilities [36–39]. In some systems this assumption is well justified [14,40], while, in others, a fully coupled optoelectronic model is necessary for qualitatively and quantitatively accurate results [16,21]. Here, a fully combined optical simulation and carrier transport analysis (c.f., EQE curves in Fig. 3a,b) indicates that photons and electrons are more efficiently collected at shorter wavelengths than at longer wavelengths in the randomly textured device. All generated carriers are collected near 550 nm, while only about 80% of generated carriers are collected at 1040 nm, given by the ratio of the absorbed photons in the CIGS and the EQE curve. Minority electrons generated near the CIGS|Mo interface are swept to the back-contact and recombine. This only occurs at longer wavelengths with correspondingly low absorption coefficients of the CIGS absorber.

The illuminated J-V curves for various underlying CIGS film thickness are shown in Fig. 4. The change in J_{SC} between the t = 700 nm and t = 1700 nm devices is 0.8 mA, cm^{-2}, and this increase is less than 3% as previously predicted by the optical analysis. In contrast the V_{OC} increases significantly, from 605.3 mV to a maximal value of 634.2 mV. The small increase in J_{SC} alone cannot account for the substantial increase of the V_{OC}. The observed V_{OC} gain is instead

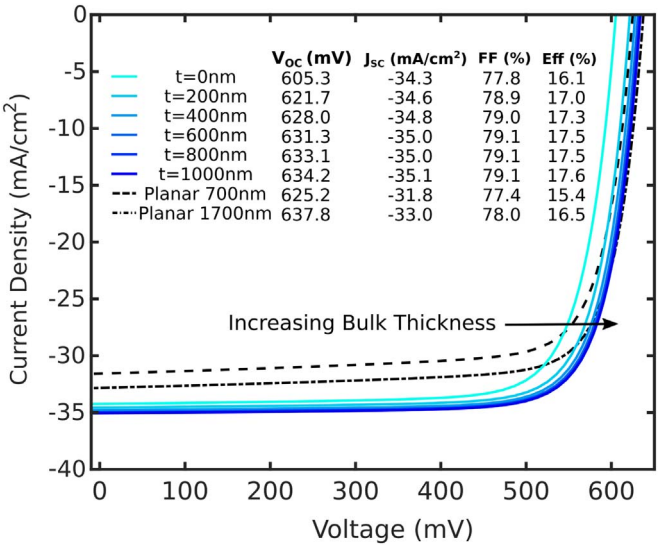

Fig. 4. (color online) Randomly Textured CIGS Photovoltaic Response Illuminated simulations of devices with varying CIGS bulk thickness, t, (c.f., inset of Fig. 2a) compared with the simulated J-V curves of equivalent planar devices. Extracted J-V parameters are given by inset.

attributed to the spatial separation of carrier generation in thicker films from parasitic recombination at the back-contact, giving minority carriers generated at depth a greater chance of diffusing to the space charge region near the diode junction [1]. The estimated bulk minority carrier diffusion length is ~700 nm, and for sufficiently thick CIGS films, the majority of photogenerated carrier are at least this distance from the back-contact, so recombination is reduced and the V_{OC} approaches a maximal value.

Here, the V_{OC} of a randomly textured device with 1 μm of underlying CIGS shows a slightly diminished VOC compared to a planar device of the equivalent 1.7 μm of material (634.2 mV and 637.8 mV respectively). This can be expected due to the increasing junction area, and therefore dark recombination. However, these simulations found the increase in current overcomes the loss in voltage when considering the overall efficiency, provided back-surface recombination is mitigated by sufficient underlying thickness. For these textured devices it is equally important that the surface recombination velocity (SRV) at the CdS|CIGS interface is kept below 10^3 cms^{-1} or the substantially increased interface area will quickly reduce device fill factor as the SRV at this interface increases (See SI2). These results encourage further investigation of this system into other potential limiting issues, including increased shunting, potentially high defect concentrations at sharp features, and this additional need to control the junction interface recombination.

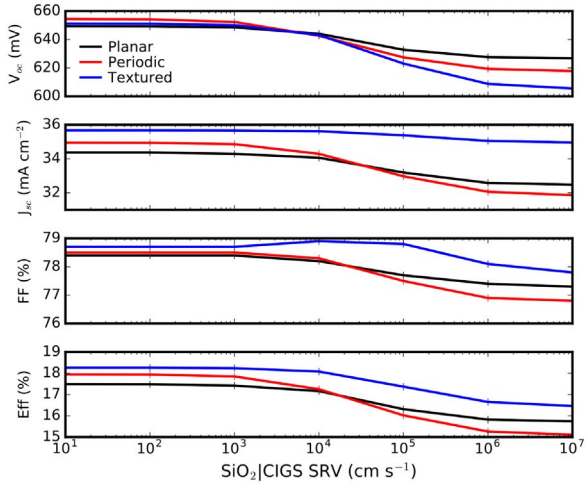

Fig. 5. Effect of Dielectric Surface Recombination V_{OC}, J_{SC}, fill factor, and efficiency of simulated devices with dielectric layers (t=0 nm for the randomly textured device) that define line contacts for parametrically varied CIGS| SiO_2 interface surface recombination velocity.

3.2.2. Electronic benefits of thin film dielectric layers

Thin film dielectric separation layers embedded between the CIGS absorber and Mo contact provide a barrier to minority carrier recombination if appropriate surface passivation can be achieved at CIGS| dielectric interfaces. SRVs in the range of 10^2 – 10^4 cms^{-1} have been reported for alumina dielectric layers, and similar values could be expected with other oxides such as silica [9,30]. Fig. 5 shows light J-V parameters of the textured device in Fig. 1c while parametrically varying the SRV at the CIGS| dielectric separation layer interfaces. The V_{OC} remains large until ~10^3 cms^{-1} and then drops monotonically for larger surface recombination velocities; similar results are seen for the J_{SC} and efficiency. The periodically structured device suffers the most in terms of J_{SC} and fill factor with this increase in SRV due to its larger interface area. The planar device maintains the most stable V_{OC}, but loses J_{SC} must faster than the randomly textured device. If low SRVs can be achieved, a line/point contact scheme with a dielectric reflection layer would represent an attractive device design to increase both the J_{SC} and V_{OC} of any thin-film device architecture [9,30]. The improvements when adding the dielectric layer are summarized in Table 1, along with the device performance when adding a MgF_2 ARC that has been optimized for photocurrent absorbed by the CIGS (SI1).

The back-contact passivation by dielectric separation layers in sub-micron thickness CIGS films is only required when a band offset exists between the CIGS and the Mo contact. A thin layer of $MoSe_2$ is sometimes used to create an indirect ohmic contact to Mo, but this has been reported to cause delamination issues in cases when this layer is excessively thick [26]. Ga grading has also been proposed to avoid minority carrier loss to the back-contact [1]. We examined the sensitivity of the randomly textured CIGS device to this offset in the Supplementary Information (SI3) and find that, electronically, adding dielectric reflection layers have a similar effect as making this offset

Table 1
Summary of JV parameters for different device configurations.

Simulated Device	V_{OC} (mV)	J_{SC} (mA cm^{-2})	FF (%)	Effciency (%)
Equivalent Thickness Planar	625.2	31.8	77.4	15.4
Periodic Structure[a]	641.0	33.6	78.5	16.9
Randomly Textured	605.3	34.3	77.9	16.1
Simulated Device with 190 nm Dielectric Layer[a]				
Equivalent Thickness Planar	648.6	34.3	78.4	17.4
Periodic Structure	652.4	34.9	78.5	17.9
Randomly Textured	654	35.2	78.4	18.1
Simulated Device with 190 nm Dielectric Layer and ARC[a]				
Equivalent Thickness Planar	653.1	37.4	78.4	19.1
Periodic Structure[b]	654.8	37.6	78.5	19.3
Randomly Textured	655.8	38.3	78.5	19.7

[a] The SRV at the CIGS|SiO2 interface is 10^3 cm s^{-1}
[b] This ARC was 166 nm instead of 110 nm.

more positive, but, optically, dielectric layers give more J_{SC} due to increased double pass absorption. Thus, sparsely arrayed line contacts are the preferred design to simultaneously minimize surface recombination and enable the required majority carrier transport while increasing double pass absorption.

Due to computational limitations, we were unable to simulate line contacts with spacing of greater than 7.8 μm. Thus the ultimate potential of the dielectric layer line contact design was not fully optimized in this study. We note that majority carriers are collected at the back-contact in this scheme, so the period of the line contacts can be on the order of the majority carrier diffusion length, as is the case here. The line contacts were 230 nm in width for all devices as in Fig. 1c,d. We observed that decreasing the contact opening could further enhance the passivation effect, indicating that recombination is not negligible even for this line contact spacing of 7.8 μm. However, very small line contacts on the order of 150 nm began to limit the J_{SC}. Additionally, experimentally contacting the Mo may be difficult with excessively small vias. We also recognize the beneficial role of Na^+ ion diffusion through the Mo back-contact should not be ignored, but incorporation of sodium fluoride into dielectric reflection layer has been reported before [12,29,30]. It is proposed first here that direct incorporation of Na^+ into a sol-gel layer used in nanoimprint fabrication could be a scalable solution to controlled Na^+ incorporation.

4. Conclusion

We report coupled optoelectronic simulations for light trapping and surface passivation in CIGS photovoltaics, and indicate designs to match or exceed the performance of thick planar absorbers. For randomly textured CIGS cells, the majority of light absorption occurs in the textured region near the junction. Long wavelength light is effectively scattered giving a flat, broadband absorption spectrum. Other light trapping strategies were examined, including dielectric separation layers located between the CIGS absorber and Mo back-contact. These layers can be designed to preferentially reflect near band-gap light back into the absorber to reduce parasitic Mo absorption. Periodic dielectric structures can also give enhancement by increasing scattering into the device. Employing various combinations of different light trapping strategies in these thin film devices demonstrates synergistic effects. For example, combining dielectric layers and periodic nanostructures gives absorption spectra characterized by superposition of these two different effects.

These optoelectronic models also addressed the other main challenge to sub-micron absorbers, namely, minority carrier recombination at the back-contact. Dielectric separation layers show the dual promises of surface passivation while enhancing double-pass absorption. Finally, we compared each device with the addition of a $\frac{1}{4}$ wavelength MgF_2 anti-reflection coating and found that a randomly textured absorber with t = 0 nm (700 nm planar equivalent) with a 190 nm dielectric separation layer shows the largest potential efficiency (see SI1). These efficiencies represent an upper bound to the CIGS architectures simulated here. Experimentally, planar devices may be easier to achieve due to the less stringent requirements on SRV of the CIGS|SiO_2 and CIGS|CdS interfaces. However, randomly or periodically structured CIGS devices with reasonably achievable CIGS|SiO_2 SRV values significantly out-performed the planar architectures. Devices utilizing this design approach could result in improved CIGS photovoltaic efficiency with a significant reduction in absorber layer thickness, and corresponding reduction in material consumption and cost.

Acknowledgments

The authors thank Hal Emmer, Chris T. Chen, Yulia Tolstova, and Stefan Olmelcheko for helpful discussions. Dr. Stanbery acknowledges the HelioVolt team of co-inventors that developed the processing technology to create these nanotextured absorbers [10]. This work was supported by the U.S. Department of Energy and the Bay Area Photovoltaic Consortium under award number DE-EE0004946 (C.R.B. and D.M.C.) and the Joint Center for Artificial Photosynthesis (KT.F. and H.A.A.), a DOE Energy Innovation Hub, supported through the Office of Science of the U.S. Department of Energy under Award No. DE-SC0004993. K.T. Fountaine was supported by the National Science Foundation Graduate Research Fellowship under Grant No DGE-1144469.

Appendix A. Supplementary data

Supplementary data associated with this article can be found in the online version at http://dx.doi.org/10.1016/j.solmat.2016.11.008.

References

[1] M. Gloeckler, J.R. Sites, Potential of submicrometer thickness Cu(In,Ga)Se2 solar cells, J. Appl. Phys. 98 (10) (2005) 103703. http://dx.doi.org/10.1063/1.2128054 URL: ⟨http://scitation.aip.org/content/aip/journal/jap/98/10/10.1063/1.2128054⟩).

[2] M.D. Kelzenberg, S.W. Boettcher, J.a. Petykiewicz, D.B. Turner-Evans, M.C. Putnam, E.L. Warren, J.M. Spurgeon, R.M. Briggs, N.S. Lewis, H.a. Atwater, Enhanced absorption and carrier collection in Si wire arrays for photovoltaic applications, Nat. Mater. 9 (4) (2010) 368. http://dx.doi.org/10.1038/nmat2727 (URL: ⟨http://www.nature.com/doifinder/10.1038/nmat2727⟩).

[3] P. Campbell, M.a. Green, Light trapping properties of pyramidally textured surfaces, J. Appl. Phys. 62 (1) (1987) 243. http://dx.doi.org/10.1063/1.339189 (URL:⟨http://scitation.aip.org/content/aip/journal/jap/62/1/10.1063/1.339189⟩).

[4] E. Yablonovitch, Statistical ray optics, J. Opt. Soc. Am. 72 (7) (1982) 899. http://dx.doi.org/10.1364/JOSA.72.000899 (URL: ⟨http://www.opticsinfobase.org/abstract.cfm?uri=josa-72-7-899⟩).

[5] H.W. Deckman, C.R. Wronski, H. Witzke, E. Yablonovitch, Optically enhanced amorphous silicon solar cells, Appl. Phys. Lett. 42 (11) (1983) 968–970. http://dx.doi.org/10.1063/1.93817.

[6] J. Müller, B. Rech, J. Springer, M. Vanecek, TCO and light trapping in silicon thin film solar cells, Sol. Energy 77 (6) (2004) 917–930. http://dx.doi.org/10.1016/j.solener.2004.03.015 (URL:⟨http://linkinghub.elsevier.com/retrieve/pii/S0038092×04000647⟩).

[7] J. Grandidier, R.a. Weitekamp, M.G. Deceglie, D.M. Callahan, C. Battaglia, C.R. Bukowsky, C. Ballif, R.H. Grubbs, H.a. Atwater, Solar cell efficiency enhancement via light trapping in printable resonant dielectric nanosphere arrays, Phys. Status Solidi (a) 210 (2) (2013) 255–260. http://dx.doi.org/10.1002/pssa.201228690.

[8] C. Colin, I. Massiot, A. Cattoni, N. Vandamme, C. Dupuis, N. Bardou, I. Gerard, N. Naghavi, J.-F. Guillemoles, J.-L. Pelouard, S. Collin, Broadband light-trapping in ultra-thin nano-structured solar cells, 2013, 86200C.URL: ⟨http://proceedings.spiedigitallibrary.org/proceeding.aspx?Doi=10.1117/12.2004269⟩ URL: ⟨http://dx.doi.org/10.1117/12.2004269⟩.

[9] C. van Lare, G. Yin, A. Polman, M. Schmid, Light coupling and trapping in ultrathin Cu(In,Ga)Se 2 solar cells using dielectric scattering patterns, ACS Nano URL: ⟨http://dx.doi.org/10.1021/acsnano.5b04091⟩

[10] B. Sang, D. Lu, R.M. Miller, C.R. Martinez, M. Kim, S.-S. Moon, B.J. Stanbery, Nanostructured CIGS Absorber Surface for Enhanced Light Trapping (2014). URL: ⟨ https://patentscope.wipo.int/search/en/WO2014028542⟩

[11] M.-C. van Lare, A. Polman, Optimized scattering power spectral density of photovoltaic light-trapping patterns, ACS Photon. (2015). http://dx.doi.org/10.1021/ph500449v (150626105810001).

[12] B. Vermang, J.T. Wätjen, V. Fjällström, F. Rostvall, M. Edoff, R. Gunnarsson, I. Pilch, U. Helmersson, R. Kotipalli, F. Henry, D. Flandre, Highly reflective rear surface passivation design for ultra-thin Cu(In,Ga)Se2 solar cells, Thin Solid Films 582 (2015) 300–303. http://dx.doi.org/10.1016/j.tsf.2014.10.050 (URL: http://linkinghub.elsevier.com/retrieve/pii/S0040609014010116).

[13] D. Callahan, K. Horowitz, H. Atwater, Light trapping in ultrathin silicon photonic crystal superlattices with randomly-textured dielectric incouplers, Opt. Express 21 (25) (2013) 4239–4245. http://dx.doi.org/10.1364/OE.21.030315 (URL:⟨http://www.opticsinfobase.org/oe/fulltext.cfm?uri=oe-21-25-30315⟩).

[14] V.E. Ferry, A. Polman, H.a. Atwater, Modeling light trapping in nanostructured solar cells, ACS Nano 5 (12) (2011) 10055–10064. http://dx.doi.org/10.1021/nn203906t (URL:⟨http://www.ncbi.nlm.nih.gov/pubmed/22082201⟩).

[15] M.G. Deceglie, V.E. Ferry, A.P. Alivisatos, H.a. Atwater, Design of nanostructured solar cells using coupled optical and electrical modeling, Nano Lett. 12 (6) (2012) 2894–2900. http://dx.doi.org/10.1021/nl300483y.

[16] X. Li, N.P. Hylton, V. Giannini, K.-H. Lee, N.J. Ekins-Daukes, S.a. Maier, Bridging electromagnetic and carrier transport calculations for three-dimensional modelling of plasmonic solar cells, Opt. Express 19 (Suppl. 4) (2011) A888–A896. http://dx.doi.org/10.1364/OE.19.00A888.

[17] M.D. Abràmoff, P.J. Magalhaes, S.J. Ram, Image processing with imageJ (2004). URL: ⟨http://biomedicaloptics.spiedigitallibrary.org/article.aspx?Doi=10.1117/1.

3589100⟩ URL: ⟨http://dx.doi.org/10.1117/1.3589100⟩
[18] M. Alonso, M. Garriga, C. Durante Rincón, E. Hernández, M. León, Optical functions of chalcopyrite CuGa x In 1-x Se 2 alloys, Appl. Phys. A: Mater. Sci. Process. 74 (5) (2002) 659–664. http://dx.doi.org/10.1007/s003390100931 (URL: ⟨http://link.springer.com/10.1007/s003390100931⟩).
[19] R.E. Treharne, A. Seymour-Pierce, K. Durose, K. Hutchings, S. Roncallo, D. Lane, Optical Design and Fabrication of Fully Sputtered CdTe/CdS Solar Cells, J. Phys.: Conf. Ser. 286 (2011) 012038. URL: ⟨http://stacks.iop.org/1742–6596/286/i=1/a=012038?Key=crossref.f72fda0fcf5aa2cd75968988273f5ce4⟩ URL: ⟨http://dx.doi.org/10.1088/1742-6596/286/1/012038⟩
[20] Sopra Materials Database URL: ⟨http://www.filmetrics.com/refractive-index-database/Mo/Molybdenum⟩.
[21] K.T. Fountaine, H.A. Atwater, Mesoscale modeling of photoelectrochemical devices: light absorption and carrier collection in monolithic, tandem, Si–WO_3 microwires, Opt. Express 22 (S6) (2014) A1453. http://dx.doi.org/10.1364/OE.22.0A1453 URL: ⟨https://www.osapublishing.org/oe/abstract.cfm?uri=oe-22-S6-A1453⟩.
[22] M. Gloeckler, A.L. Fahrenbruch, J.R. Sites, Numerical modeling of CIGS and CdTe solar cells: setting the baseline, in: Proceedings of 3rd World Conference onPhotovoltaic Energy Conversion, 2003.
[23] I. Repins, S. Glynn, J. Duenow, T.J. Coutts, W.K. Metzger, M.A. Contreras, Required Material Properties for High-Efficiency CIGS Modules, no. July 2009, pp. 74090M–74090M–14. URL: ⟨http://proceedings.spiedigitallibrary.org/proceeding.aspx?Articleid=1340399⟩ URL: ⟨http://dx.doi.org/10.1117/12.828365⟩.
[24] N. Dahan, Z. Jehl, T. Hildebrandt, J.-J. Greffet, J.-F. Guillemoles, D. Lincot, N. Naghavi, Optical approaches to improve the photocurrent generation in Cu(In,Ga)Se2 solar cells with absorber thicknesses down to 0.5 μm, J. Appl. Phys. 112 (9) (2012) 094902. http://dx.doi.org/10.1063/1.4762004 (URL: ⟨http://scitation.aip.org/content/aip/journal/jap/112/9/10.1063/1.4762004⟩).
[25] K. Orgassa, H. Schock, J. Werner, Alternative back contact materials for thin film Cu(In,Ga)Se2 solar cells, Thin Solid Films 431–432 (03) (2003) 387–391. http://dx.doi.org/10.1016/S0040-6090(03)00257-8 (URL: ⟨http://linkinghub.elsevier.com/retrieve/pii/S0040609003002578⟩).
[26] B.J. Stanbery, Copper indium selenides and related materials for photovoltaic devices, Crit. Rev. Solid State Mater. Sci. 27 (2) (2002) 73–117. http://dx.doi.org/10.1080/20014091104215 (URL: ⟨http://www.tandfonline.com/doi/abs/10.1080/20014091104215⟩).
[27] M.A. Contreras, M.J. Romero, B. To, F. Hasoon, R. Noufi, S. Ward, K. Ramanathan, Optimization of CBD CdS process in high-efficiency Cu(In,Ga)Se2-based solar cells, in: Thin Solid Films, Vol. 403-404, 2002, pp. 204–211. URL: ⟨http://dx.doi.org/10.1016/S0040-6090(01)01538-3⟩.
[28] N. Naghavi, D. Abou-Ras, N. Allsop, N. Barreau, S. Bücheler, A. Ennaoui, C.H. Fischer, C. Guillen, D. Hariskos, J. Herrero, R. Klenk, K. Kushiya, D. Lincot, R. Menner, T. Nakada, C. Platzer-Björkman, S. Spiering, A.N. Tiwari, T. Törndahl, Buffer layers and transparent conducting oxides for chalcopyrite Cu(In,Ga)(S, Se)2 based thin film photovoltaics: present status and current developments, Prog. Photovolt.: Res. Appl. 18 (6) (2010) 411–433. http://dx.doi.org/10.1002/pip.955.
[29] B. Vermang, J.T. Wätjen, V. Fjällström, F. Rostvall, M. Edoff, R. Kotipalli, F. Henry, D. Flandre, Employing Si solar cell technology to increase efficiency of ultra-thin Cu(In,Ga)Se 2 solar cells, Prog. Photovolt.: Res. Appl. 22 (10) (2014) 1023–1029. http://dx.doi.org/10.1002/pip.2527 (URL: http://dx.doi.org/doi:10.1002/pip.1160 http://doi.wiley.com/10.1002/pip.2527).
[30] B. Vermang, V. Fjällström, J. Pettersson, P. Salomé, M. Edoff, Development of rear surface passivated Cu(In,Ga)Se2 thin film solar cells with nano-sized local rear point contacts, Sol. Energy Mater. Sol. Cells 117 (2013) 505–511. http://dx.doi.org/10.1016/j.solmat.2013.07.025 (URL: ⟨http://linkinghub.elsevier.com/retrieve/pii/S0927024813003711⟩).
[31] M.A. Verschuuren, Substrate Conformal Imprint Lithography for Nanophotonics, Ph.D. thesis, Utrecht University, 2010.
[32] M. Verschuuren, H. Sprang, 3D photonic structures by sol-gel imprint lithography, MRS Proc. 1002 (2007) 1–6 (URL:⟨ http://journals.cambridge.org/abstract_S1946427400596456⟩).
[33] M.D. Kelzenberg, Appendix B: Silicon Microwire Photovoltaics, Ph.D. thesis, California Institute of Technology, 2010.
[34] V.E. Ferry, Light trapping in plasmonic solar cells, Ph.D. thesis, California Institute of Technology, 2011. URL: ⟨http://www.ncbi.nlm.nih.gov/pubmed/20588593⟩
[35] C. van Lare, F. Lenzmann, M.a. Verschuuren, A. Polman, Dielectric scattering patterns for efficient light trapping in thin-film solar cells, Nano Lett. (2015). http://dx.doi.org/10.1021/nl5045583 (150630085420008).
[36] P. Wang, R. Menon, Optimization of periodic nanostructures for enhanced light-trapping in ultra-thin photovoltaics, Opt. Express 21 (5) (2013) 6274. http://dx.doi.org/10.1364/OE.21.006274 (URL: ⟨http://www.ncbi.nlm.nih.gov/pubmed/23482196⟩).
[37] Q.G. Du, C.H. Kam, H.V. Demir, H.Y. Yu, X.W. Sun, Enhanced optical absorption in nanopatterned silicon thin films with a nano-cone-hole structure for photovoltaic applications, Opt. Lett. 36 (9) (2011) 1713. http://dx.doi.org/10.1364/OL.36.001713 (URL: ⟨https://www.osapublishing.org/ol/abstract.cfm?uri=ol-36-9-1713⟩).
[38] A. Oskooi, P.a. Favuzzi, Y. Tanaka, H. Shigeta, Y. Kawakami, S. Noda, Partially disordered photonic-crystal thin films for enhanced and robust photovoltaics, Appl. Phys. Lett. 100 (18) (2012) 181110. http://dx.doi.org/10.1063/1.4711144.
[39] L. Ji, W.J. Nam, S. Fonash, Highly ordered nano-cone back reflector arrays for ultra-thin high performance CIGS cells, in: 2013 IEEE 39th Photovoltaic Specialists Conference (PVSC), IEEE, 2013, pp. 1977–1979. URL: ⟨http://ieeexplore.ieee.org/lpdocs/epic03/wrapper.htm?arnumber=6744858⟩, http://dx.doi.org/10.1109/PVSC.2013.6744858.
[40] L. Yang, L. Mo, Y. Okuno, S. He, Optimal design of ultrabroadband, omnidirectional, and polarizationinsensitive amorphous silicon solar cells with a coreshell nanograting structure, Prog. Photovolt. (2013) 1077–1086. http://dx.doi.org/10.1002/pip (URL: http://onlinelibrary.wiley.com/doi/10.1002/pip.2206/full).